Journal of Natural Gas Science and Engineering 50 (2018) 181–188

Contents lists available at ScienceDirect

Journal of Natural Gas Science and Engineering

journal homepage: www.elsevier.com/locate/jngse

Selective adsorption of supercritical carbon dioxide and methane binary mixture in shale kerogen nanopores

Tianyu Wang, Shouceng Tian*, Gensheng Li, Mao Sheng

State Key Laboratory of Petroleum Resources and Prospecting, China University of Petroleum, Beijing 102249, China

ARTICLE INFO

Keywords:
Methane
Kerogen
Supercritical carbon dioxide
Selective adsorption
Molecular simulation

ABSTRACT

The adsorption of carbon dioxide and methane binary mixture in shale kerogen nanopores and the underlying mechanism significantly affect the supercritical carbon dioxide enhanced shale gas development project. In this study, we investigated the adsorption properties of carbon dioxide and methane in shale kerogen using grand canonical Monte Carlo (GCMC) method. Shale kerogen was fabricated based on Ungerer molecular model and its parameters were validated. The effects of temperature, pressure, mole fraction on the adsorption isotherms, average isosteric heat, potential energy distribution, and adsorption selectivity of binary mixture were discussed. The results show that the absolute adsorption capacity of methane in binary mixture decreases as temperature increases, but increases as mole fraction increases. Compared with methane, carbon dioxide is in lower energy absorption sites, which indicates the adsorption capacity of carbon dioxide in shale kerogen is stronger than that of methane. The adsorption selectivity of carbon dioxide over methane first decreases as pressure increases until pressure reaches critical pressure (7.38 MPa for carbon dioxide), and then stays at around 3.8 as pressure continues to rise. Adsorption selectivity and desorption quantity are used to reveal that the optimal injection depth for supercritical carbon dioxide enhanced shale gas development project is 1000–2500 m. This study will reveal the mechanism of the adsorption of methane in kerogen and provide some fundamental data for supercritical carbon dioxide enhanced shale gas development project.

1. Introduction

Energy crisis and carbon emission have become a hot topic that attracts global attention. Shale gas, as a kind of clean and efficient resource, is an important alternative to conventional fossil energy (Boyer et al., 2011; Ren et al., 2016; Siirola, 2014). Nowadays, injecting carbon dioxide into geological structures for storage is considered as an important method for reducing carbon emission and mitigating global warming, especially as conventional fossil fuels are still the major energy consumed around the world (Kang et al., 2011; Kharaka et al., 2006). Therefore, using carbon dioxide to enhance shale gas development brings benefit for shale gas exploitation and carbon dioxide geological storage.

Methane, the main component of shale gas, is either in free state, adsorbed state or dissolved state in shale gas reservoirs. The free gas mainly exists in nanopores in shale kerogen and among mineral grains in shale gas reservoirs, whereas adsorbed gas exists on the surface of the organic matters in shale gas reservoirs (Heller and Zoback, 2014; Howarth et al., 2011; Xiong et al., 2017). The percentage of shale gas in absorbed phase ranges from 20% to 85% of the total gas-in-place (Curtis, 2002). It is believed that shale gas in adsorption phase is highly related to the organic matters, while other compositions, such as clay minerals, have less contribution to methane adsorption in organic-rich shale (Chalmers and Bustin, 2007; Gasparik et al., 2014; Ren et al., 2017a). Also, carbon dioxide is in the supercritical state under certain geological conditions. Supercritical carbon dioxide (SC-CO2) enhanced shale gas development project has many unique advantages for the exploitation of shale resources, and is expected to become a novel technique to help shale gas development (Bennion and Bachu, 2008; Lee et al., 2016; Wang et al., 2016; Weniger et al., 2010). As commonly expected, majority of measurements showed that preferential adsorption of carbon dioxide over methane (Ambrose et al., 2011; Billemont et al., 2010; Brochard et al., 2012; Collell et al., 2015; Howarth et al., 2011; Liu and Wilcox, 2012; Ren et al., 2017b). However, there have been a limited number of experimental studies on adsorption of gas mixtures in shale kerogen (Heller and Zoback, 2014), the behavior of kerogen in response to supercritical carbon dioxide injection is still not well understood due to the complexity of the shale kerogen structure and associated geological conditions. Therefore, understanding the adsorption selectivity and behavior of carbon dioxide and methane

* Corresponding author.
E-mail address: tscsydx@cup.edu.cn (S. Tian).

https://doi.org/10.1016/j.jngse.2017.12.002
Received 22 September 2017; Received in revised form 7 December 2017; Accepted 10 December 2017
Available online 19 December 2017
1875-5100/

binary mixture in shale kerogen is critical for shale gas resource assessment and shale gas recovery.

Kerogen is generally defined as the fraction of sedimentary organic matter that is insoluble in common polar solvents (Behar and Vandenbroucke, 1987; Durand, 1980), depending on its origin and degree of thermal alteration that make up a portion of the organic matter. Modeling mixture adsorption on kerogen is not a trivial work due to its chemical heterogeneity. To our best knowledge, there is little research on competitive adsorption of CH_4 and CO_2 on different kerogens (Bousige et al., 2016). Previous studies have shown that the amount and type of organic matter influence the methane adsorption capacity of shale, as does moisture content, pressure, and temperature (Chalmers and Bustin, 2008; Weniger et al., 2010; Zhang et al., 2012). In addition, Collell et al. (2014). used molecular simulations to study the structural and physical properties of kerogen in shale formation. Falk et al. (2015). used molecular simulations to investigate the adsorption behavior and structure of n-alkanes in kerogen. The adsorption follows Langmuir-type adsorption isotherm due to the nanopores size of kerogen. Bousige et al. (2016). used a hybrid experimental simulation method to investigate essential characteristics of kerogen such as pore distribution, stiffness and vibrational density of states.

In recent years, molecular simulation has become a new approach in addition to theoretical and experimental methods in the study of microscopic phenomenon (Collell et al., 2015; Frenkel and Smit, 2001; McGreevy and Pusztai, 1988). It is commonly applied in the study of molecular adsorption in porous media, such as the molecular sieve adsorption (Granato et al., 2008), metal organic frameworks (Yaghi et al., 2003) and carbon nanotubes (Mao and Sinnott, 2000). Billemont et al. (2010). studied the effect of water on the adsorption of methane in nanopores using molecular simulation methods, which indicated that the presence of water decreased the adsorption capacity of methane. Lu et al. (2015). studied the effect of different functional groups on the adsorption of methane and carbon dioxide by GCMC methods, which indicated that the different functional groups had a significant influence on the adsorption of carbon dioxide. Zhao (Zhao et al., 2017) studied the adsorption capacity of methane on dry kerogen and moist kerogen, which indicated that the presence of the moisture content sharply decreases methane adsorption capacity and has a greater effect on kerogen with high maturity than on kerogen with low maturity. Research on the behavior of methane adsorption in response to supercritical carbon dioxide injection under geological conditions is still lacking.

In this study, a realistic kerogen molecular model was built, which included carbon (C), hydrogen (H), oxygen (O), nitrogen (N), and sulfur (S) atoms. We used the grand canonical Monte Carlo (GCMC) method and molecular dynamics (MD) method to investigate the adsorption behavior of methane and carbon dioxide binary mixture in shale kerogen nanopores. The impacts of temperature, the average isosteric heats and the potential energy distribution on the adsorption behaviors of methane were investigated. Finally, the adsorption selectivity and optimization of injection depth for supercritical carbon dioxide enhanced shale gas development were discussed. The results might provide theoretical and instructional significance for the exploration and development of shale gas reservoirs.

2. Models and methods

2.1. Molecular model of kerogen

The molecular model of kerogen used in this work was developed by Ungerer et al. (2014). based on analytical data from Kelemen et al. (2007). The sample of kerogen is found in the Green River Shales formation and is classified as immature based on its hydrocarbon generation. The composition is $C_{252}H_{294}O_{24}N_6S_3$. The molecular model of kerogen is illustrated in Fig. 1(a). The composition and structural parameters of the model have an excellent match with the results of the X-ray and Solid-State ^{13}C Nuclear Magnetic Resonance (NMR) data. Table 1 shows the referred parameters of the model established in this article.

10 kerogen molecules were used to build the amorphous cell with periodicity in three directions. Organic pores are shown in Fig. 1 (b). Simulated cell of kerogen is sliced paralleling three planes, respectively. In each slices, the pores are depicted in blue color. The cell was minimized by annealing dynamics with a temperature cycle from 300 K to 1000 K. The final structure of kerogen was shown in Fig. 1(c). The evolution of kerogen density in the annealing dynamics process is plotted in Fig. 1(d). The equilibrium density is 1.125 g/cm^3, which is in agreement with the measured result between 1.0 g/cm^3 and 1.15 g/cm (Mastalerz et al., 2012).

2.2. Molecular simulations

The grand canonical Monte Carlo (GCMC) method was carried out by the Sorption module in Materials Studio software. We adopted the Compass force field (Sun, 1998). The equilibrium steps were 3×10^6 and the production steps were 3×10^6. The exchange, conformation, rotation and translation in each attempted simulation were 40%, 20%, 20% and 20%. Moreover, we used the Ewald method to describe the electrostatic interactions. The van der Waals (vdW) interactions were calculated within a cutoff distance of 1.55 nm by the atom-based method. Interactions between kerogen and shale gas molecules were described using the L-J potential:

$$E(r_{ij}) = 4\varepsilon_{ij}\left[(\sigma_{ij} / r_{ij})^9 - (\sigma_{ij} / r_{ij})^6\right] \quad (1)$$

The Lorentz– Berthelot mixing rules were used to calculate cross interactions:

$$\sigma_{ij} = (\sigma_{ii} + \sigma_{jj})/2 \quad (2)$$

$$\varepsilon_{ij} = \sqrt{\varepsilon_{ii} \times \varepsilon_{jj}} \quad (3)$$

where r_{ij} is the separation of the pair of atoms i and j, ε_{ij} is the depth of the potential well, σ_{ij} is the finite distance at which the inter-particle potential is zero and r_{ij} is the distance between the particles. σ_{ii} is the diameter parameter of the adsorbate molecules and σ_{jj} is the intermolecular distances, ε_{ii} and ε_{jj} are the interaction energy of atoms i and j. Equilibrium was obtained when the number of methane and carbon dioxide molecules adsorbed in kerogen nanopores reached a constant value. The potential model used for the methane molecule is the TraPPE model (Martin and Siepmann, 1998), and the carbon dioxide molecule is simulated by the EPM2 model (Harris and Yung, 1995) which includes the bond-bending potential, the short-range LJ potential, and the long-range Coulomb potential.

In the grand canonical Monte Carlo simulation, chemical potential, volume and temperature are independent variables. The chemical potential is a function of fugacity rather than pressure. The Peng-Robinson equation is used to calculate the fugacity of CH_4 and CO_2 (Poling et al., 2001). Fig. 2 shows that with the increasing of pressure, fugacity coefficients of methane and carbon dioxide decrease gradually. It indicates deviations of fugacity from pressure rising with increasing pressure. Moreover, with increasing temperature, the fugacity coefficient increases.

3. Results and discussion

3.1. Kerogen model validation

We compared our simulation results with the experimental data from literature to validate the model and simulation method. The GCMC simulation gives absolute adsorption capacity while laboratory experiments measure excess adsorption capacity. Therefore, we used the following equation to calculate the excess adsorption isotherms and compare the simulation results with the experimental results (Gibbs,

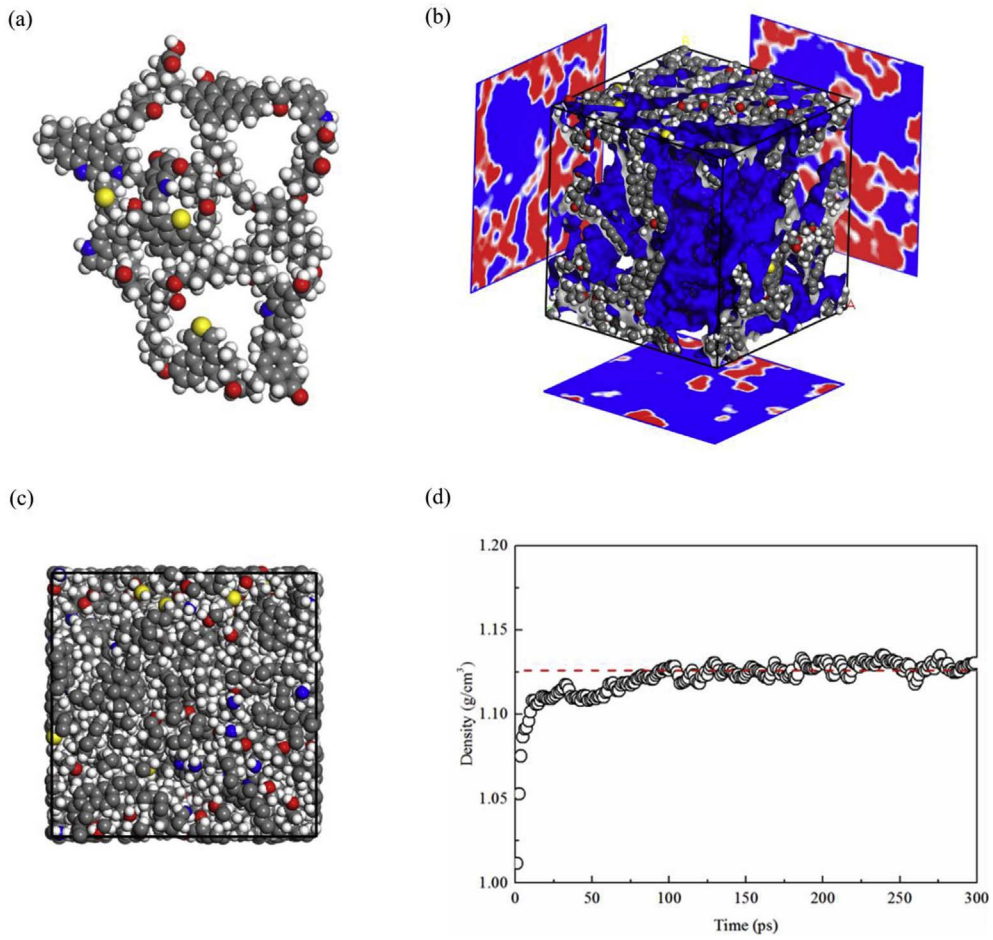

Fig. 1. (a) Kerogen molecular model in this study developed by Ungerer et al. (b) Simulated cell of kerogen with slices paralleling to AB plane, AC plane, and BC plane, respectively. In slices, the pores are depicted in blue color. (c) Shale kerogen with 10 building blocks. (d) Evolution of kerogen density in the annealing dynamic process. Color scheme: red, blue, yellow, grey, and white spheres represent oxygen, nitrogen, sulfur, carbon, and hydrogen atoms, respectively. (For interpretation of the references to color in this figure legend, the reader is referred to the Web version of this article.)

Table 1
The parameter of molecular model unit of kerogen.

Property	Quantity
H/C	1.17
O/C	0.095
N/C	0.024
S/C	0.012
% of aromatic carbon	41%
average number of C atoms per aromatic cluster	11.4
protonated aromatic C (per 100 C)	14
number of O in C−O per 100 C	5.2
number of O in (−COOH) per 100 C	1.6

1928):

$$n_{ex} = n_{ab} - \rho V/M \quad (4)$$

where n_{ex} is the excess adsorption, mol/kg; n_{ab} is the absolute adsorption, mol/kg; the V is the pore volume, m^3/kg; the ρ is the equilibrium density of methane calculated using the Peng-Robinson equation, kg/m^3; M is the molar mass of the gas, kg/mol; The experimental data used for comparison are from Alum and Barnett shale measured by Gasparik et al. (2014). The simulated data matches well with experimental data, which validates our model and GCMC simulation (see Fig. 3). The experimental data are used to fit the Langmuir model and there are differences in the maximum Langmuir sorption capacity. This is probably because that, the effects of thermal maturity plays an important role in the adsorption capacity according to the laboratory studies by Lu et al. (2015). As the clay minerals contribute little to the methane adsorption capacity in organic-rich shale (Gasparik et al., 2014), the excess adsorption of methane in kerogen can provide approximate values for the adsorption capacity in organic-rich shale.

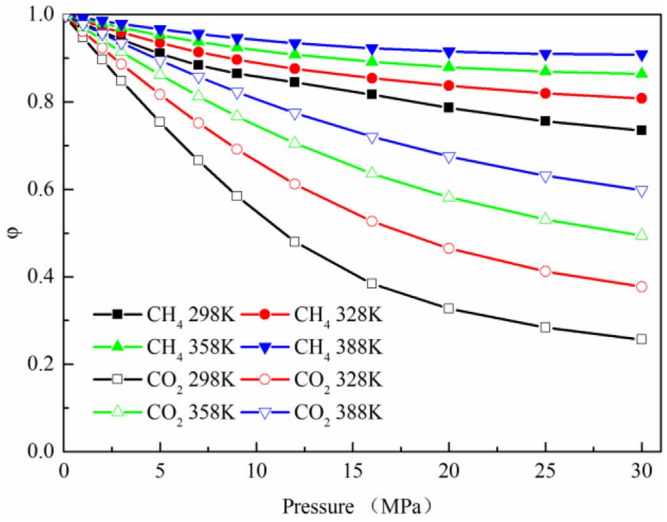

Fig. 2. The fugacity coefficient of methane for binary mixture at different temperatures and pressures.

3.2. Adsorption isotherms for the binary mixture

The adsorption isotherms of carbon dioxide and methane for different methane mole fractions at the temperature of 298 K are displayed in Fig. 4(a) and (b). It shows that for the binary mixtures, the adsorption capacity of carbon dioxide and methane in shale kerogen increases

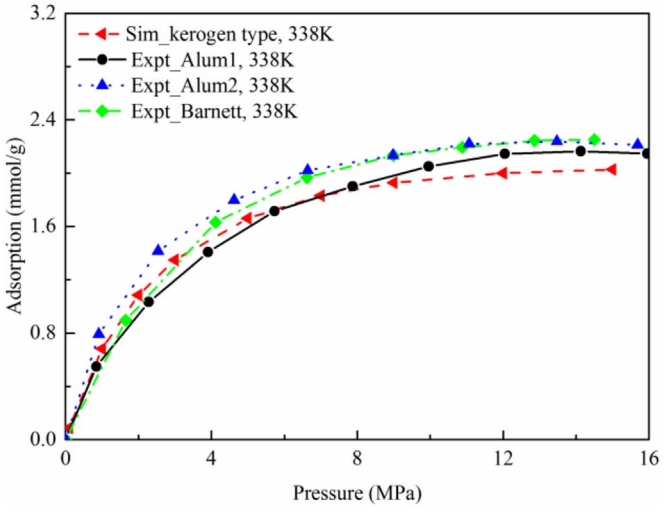

Fig. 3. Comparison of the excess adsorption capacity of methane on shale samples between simulation results and experimental results.

as its mole fraction increases. The adsorption isotherms of carbon dioxide reach its saturation adsorption under lower pressure, indicating that carbon dioxide is adsorbed in kerogen nanopores faster than that of methane. With the decrease of carbon dioxide mole fraction, the adsorption capacity of carbon dioxide decreases uniformly. The adsorption capacity of methane increases with pressure and increases faster at lower pressure. For a mixture with methane mole fraction of 0.75, the methane adsorption amount is about half of that of pure methane. The adsorption amount of methane decreases 0.45 times when the methane mole fraction decreases from 0.5 to 0.25, which indicates that the adsorption capacity decreases faster when mole fraction of methane is relatively high. In the supercritical carbon dioxide enhanced shale gas development project, a larger number of adsorbed shale gas is desorbed into free state in the early period of carbon dioxide injection. With the increases of carbon dioxide injection, desorption amount of adsorbed methane gradually decreases, which indicates that the injection of supercritical carbon dioxide will increase shale gas production in a very short time.

The adsorption isotherms of methane for methane with 0.5 and 0.75 mol fraction in shale kerogen at 298, 328, 358, 388 and 418 K were simulated to study the effects of the temperature. It can be seen in Fig. 4(c) and (d) that the absolute adsorption capacity of methane decreases as temperature increases, which indicates that higher temperature restricts methane adsorption. At the same time, low temperature facilitates methane adsorption in shale kerogen nanopores. One possible reason would be that the methane adsorption in shale kerogen is physical adsorption (Gasparik et al., 2014; Rexer et al., 2014; Zhang et al., 2012). As temperature increases, thermal motion of methane molecules increases, leading to an increase of the mean kinetic energy of the methane molecules, which would make the methane conquer the layer barrier and escape from the walls easier (Fujita et al., 2007). This is consistent with the results of the isothermal adsorption

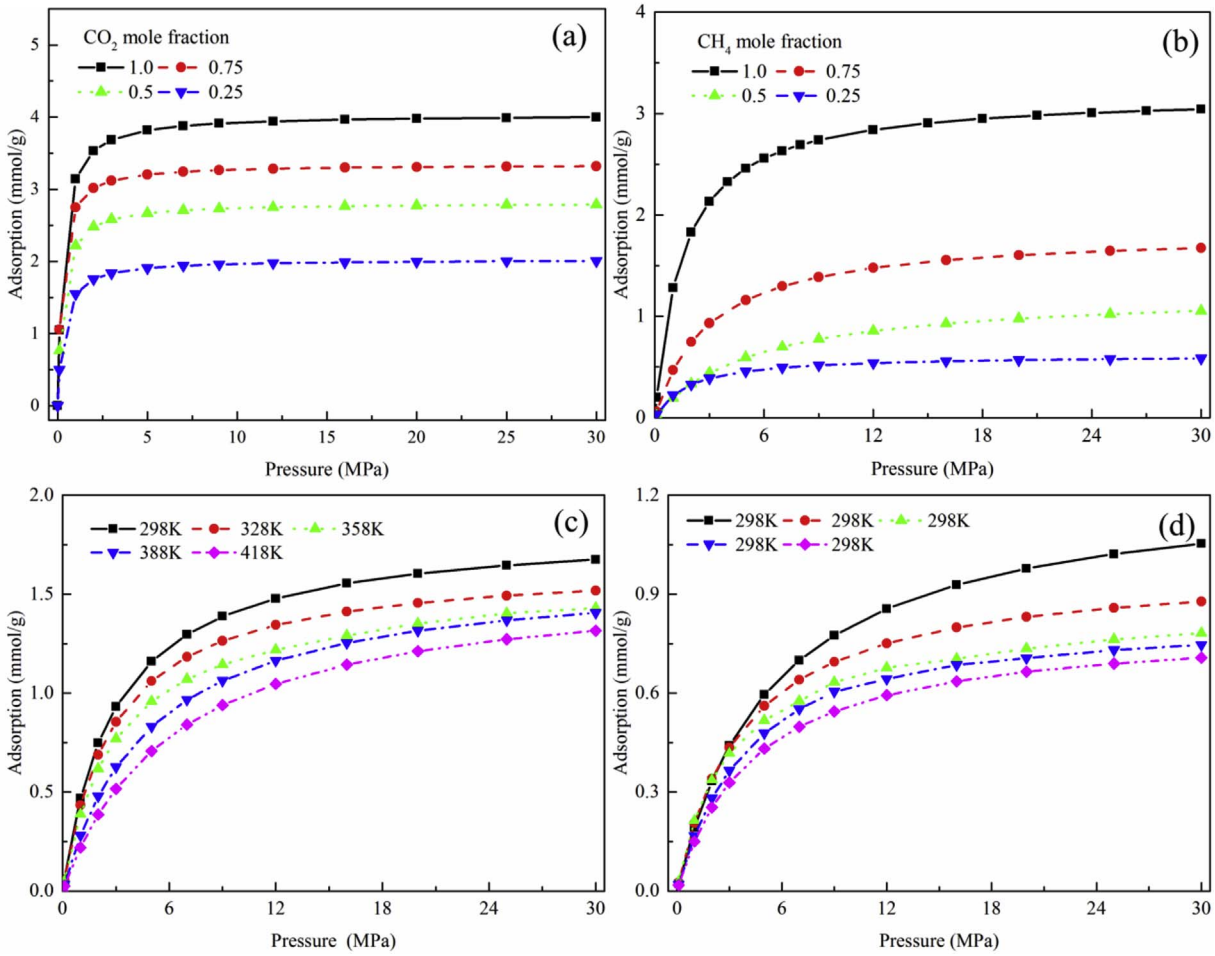

Fig. 4. (a) Adsorption isotherms of carbon dioxide for different carbon dioxide mole fractions. (b) Adsorption isotherms of methane for different methane mole fractions. (c) Adsorption isotherms of methane for methane mole fraction of 0.75 in shale kerogen at 298, 328, 358, 388 and 428 K. (d) Adsorption isotherms of methane for methane with 0.5 mol fraction in shale kerogen at 298, 328, 358, 388 and 428 K.

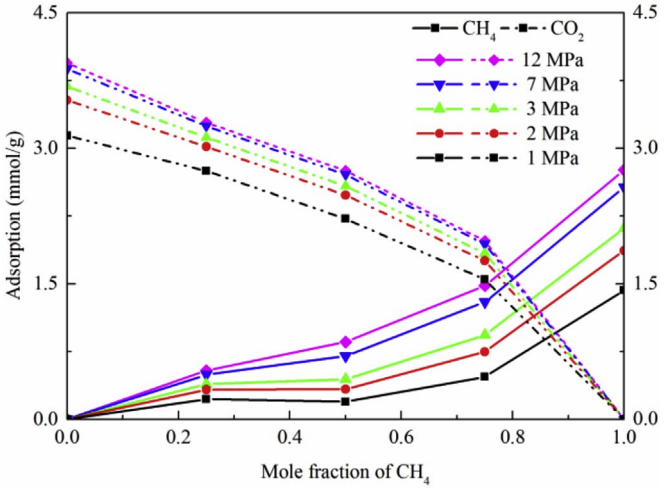

Fig. 5. Absolute adsorption of CH_4 and CO_2 for different CH_4 mole fractions at 298 K in specified pressures. For the sake of simplicity, we only show the pressures of 1, 2, 3, 7 and 12 MPa.

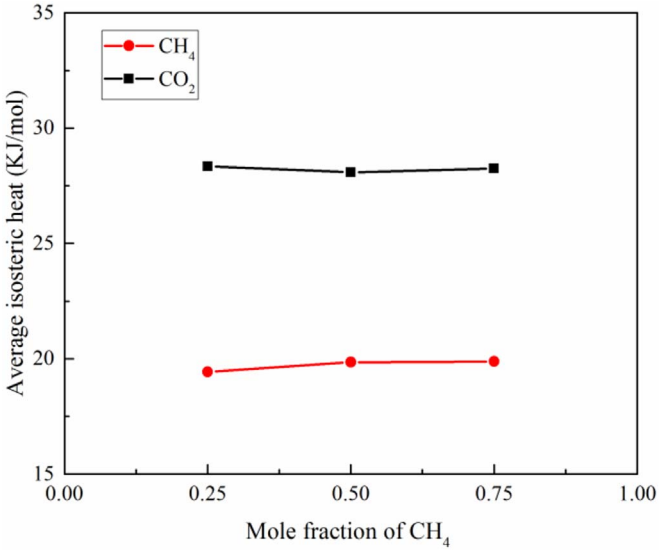

Fig. 6. The average isosteric heat of adsorption of CH_4 and CO_2 at different CH_4 mole fraction.

made by Rexer et al. (2013), suggesting that methane adsorption capacity in kerogen decreases with increasing temperature.

In order to investigate the effect of pressure on the binary mixture adsorption of carbon dioxide and methane in shale kerogen, the absolute adsorption of methane and carbon dioxide for the temperature of 298 K as a function of pressure and methane mole fraction respectively are shown in Fig. 5. It shows that higher the pressure of methane and carbon dioxide, greater the adsorption amount of carbon dioxide and methane is. As expected, carbon dioxide is preferentially adsorbed to kerogen than methane. The absolute amount of carbon dioxide adsorbed in kerogen nanopores exceeds that of methane for all pressure once carbon dioxide mole fraction is above 0.19. The adsorbed amount of carbon dioxide in kerogen increases as mole fraction of carbon dioxide increases (Zhang et al., 2015). When pressure increases from 1 MPa to 12 MPa, the bulk CH_4 mole fraction, which gives the equal adsorbed amount of CH_4 and CO_2 and above the point the amount of CO_2 adsorbed exceeds that of CH_4, shifts from 0.84 to 0.79.

3.3. Average isosteric heat and potential energy distribution

Isosteric heat of adsorption for mixture binary determine the temperature change caused by adsorption and desorption in the energy balance (Mofarahi and Bakhtyari, 2015). The average isosteric heat of methane and carbon dioxide in shale kerogen nanopores for different CH_4 mole fraction are presented in Fig. 6. It can be seen from that the isosteric heat of CO_2 is larger than that of CH_4 at different CH_4 mole fraction. The tendance are consistent with previously reported results (Billemont et al., 2013; Falk et al., 2015). Specifically, the isosteric heat of CO_2 is 28.34 kJ/mol, 28.08 kJ/mol, 28.26 kJ/mol whereas that of CH_4 is 19.43 kJ/mol, 19.84 kJ/mol, 19.87 kJ/mol, respectively, which indicates that the CH_4 and CO_2 adsorption in shale belong to physisorption. This order is consistent with the order of methane and carbon dioxide adsorption capacity at different temperatures. The isosteric heat of adsorption of methane could reflect the methane adsorption capacity to a certain extent (Xiong et al., 2017; Zhang et al., 2012). The isosteric heat of CO_2 is larger than that of CH_4 in kerogen, indicating that the kerogen models have a higher affinity for CO_2 compared with CH_4 (Huang et al., 2018). This further demonstrates that the CO_2 molecule has stronger adsorption capacity in kerogen nanopores compared with CH_4.

The potential energy distribution of methane and carbon dioxide of different methane mole fraction in shale kerogen nanopores can be directly obtained from the simulation results. The potential energy distribution curves of methane and carbon dioxide under different temperature at 30 MPa are shown in Fig. 7. The potential energy distribution follows the same trend as different mole fraction of carbon dioxide and methane binary mixture in shale kerogen. The peak positions of the curves gradually moves to the right as temperature increases, which suggests that the adsorption sites of methane molecules in shale kerogen nanopores gradually change from lower energy absorption sites to higher energy adsorption sites as temperature increases. The adsorption state of the methane in kerogen under low pressure is not as stable as that under high pressure. At the same time, as different mole fraction of carbon dioxide and methane binary mixture, the peak positions of methane is in the right of the curves of carbon dioxide, indicating that methane in shale kerogen nanopores is in the higher energy absorption sites whereas carbon dioxide is in the lower energy ones. That is to say, the adsorption capacity of carbon dioxide in shale kerogen nanopores is stronger than that of methane. This result is consistent with the fact for bituminous coal (Gensterblum et al., 2013).

3.4. Adsorption selectivity of carbon dioxide over methane

Adsorption selectivity is ued as a criterion to assess the performance of a sorbent in preferentially adsorbing species for binary mixture. It represents the ratio of the mole fractions of the two species in adsorbed phase relative to the ratio of the mole fractions in bulk phase. Adsorption selectivity greater than one indicates that the preferential adsorption of the component is greater than that of the other component in the binary mixture. The adsorption selectivity of carbon dioxide over methane in shale kerogen nanopores is defined as follows:

$$S_{CO_2} = \frac{(x_{CO_2}/x_{CH_4})_{\text{adsorbed}}}{(x_{CO_2}/x_{CH_4})_{\text{bulk}}} \tag{5}$$

where x_{CO2} and x_{CH4} denote the average mole fraction of component carbon dioxide and methane, and the subscripts ( )adsorbed and ( )bulk refer to the quantities of adsorbed phase and bulk phases, respectively.

The adsorption selectivity of carbon dioxide over methane in shale kerogen nanopores is depicted in Fig. 8. All measured adsorption selectivity values are greater than one, which indicates that carbon dioxide is preferentially adsorbed over methane under competitive adsorption conditions. Fig. 8(a) displays the adsorption selectivity of carbon dioxide over methane in shale kerogen at different methane mole fractions specified at the temperature of 328 K. The adsorption selectivity of carbon dioxide over methane first decreases as pressure

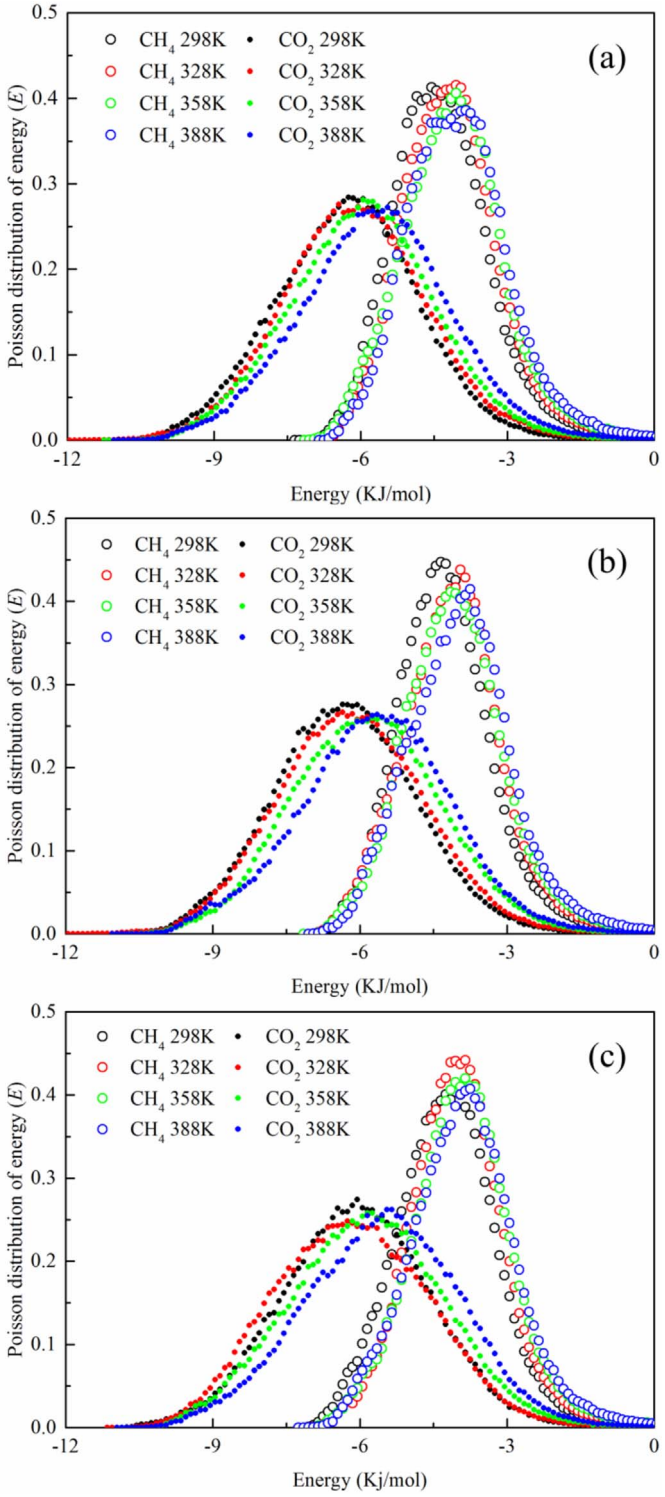

Fig. 7. The potential energy distribution curves of methane and carbon dioxide in shale kerogen under different temperature at 30 MPa. (a) The methane mole fraction is 0.75; (b) The methane mole fraction is 0.5; (c) The methane mole fraction is 0.25.

increases until the pressure reaches the critical pressure (7.38 MPa for carbon dioxide), and then stays at around 3.8 as pressure continues to rise, indicating that carbon dioxide is preferentially adsorbed in kerogen nanopores compared to methane at all different pressure. When methane is present in very low concentrations and pressure is low (0–7.38 MPa), carbon dioxide adsorption is extremely dominant. The implication of the results is that for the same amount of carbon dioxide injected, more methane is recovered in shallow sites of shale formation

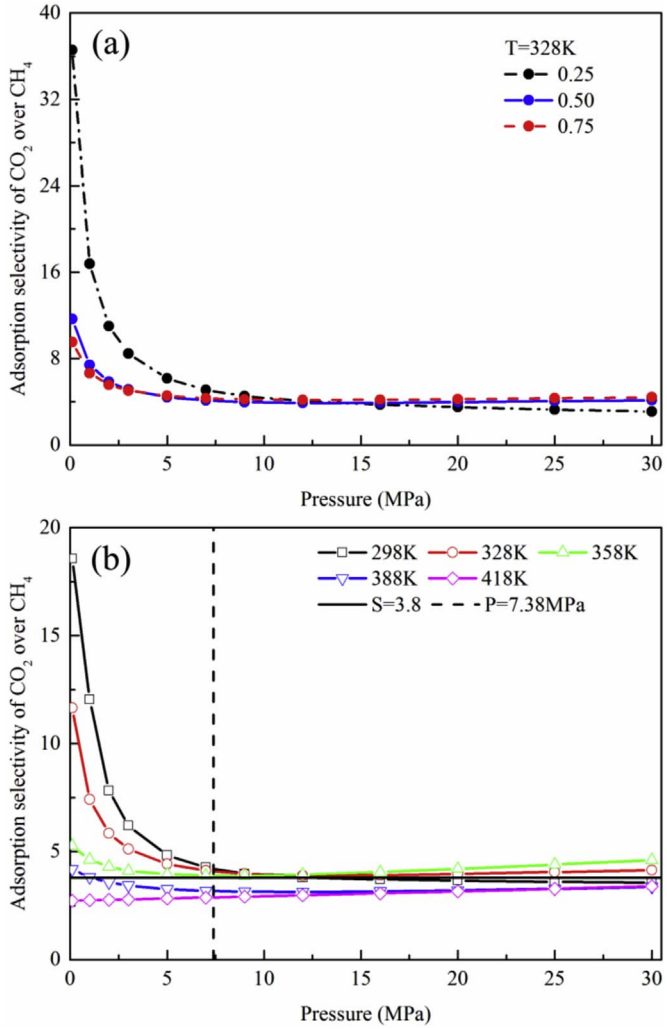

Fig. 8. Adsorption selectivity of CO2 over CH4 as a function of pressure and mole fraction of CO2: (a) at T = 328 K; (b) at (xCO2) bulk = 0.5.

than in deep ones. The adsorption selectivity of carbon dioxide over methane in shale kerogen at 298, 328, 358, 388 and 418 K are simulated to study the effects of the temperature. As shown in Fig. 8(b), the adsorption selectivity of carbon dioxide over methane decreases as temperature increases, which can be ascribed to the fact that the adsorption capacity of carbon dioxide decreases faster than that of methane at the elevated temperature. The reduction of the mole fraction of methane, the decrease of adsorption space of methane, and the change of adsorption sites of methane generate a decrease of the methane adsorption capacity for the carbon dioxide and methane binary mixture.

3.5. Optimization of injection depth for carbon dioxide

For supercritical carbon dioxide enhanced shale gas development project, carbon dioxide is pumped into injection well and entered the shale reservoir first, and it diffuses in kerogen pores until it is delivered to the adsorption sites. Carbon dioxide is in the supercritical state under geological conditions. Then, because of the preferential adsorption behavior of carbon dioxide, carbon dioxide replaces methane molecules on the adsorption sites of kerogen surface, and methane is desorbed from the shale kerogen surface. At the same time, some carbon dioxide molecules are not adsorbed in shale kerogen, and they will continue to diffuse and finally be delivered out of kerogen nanopores with the desorbed methane molecules. Finally, methane will be extracted from the released mixture species, and residual carbon dioxide will be

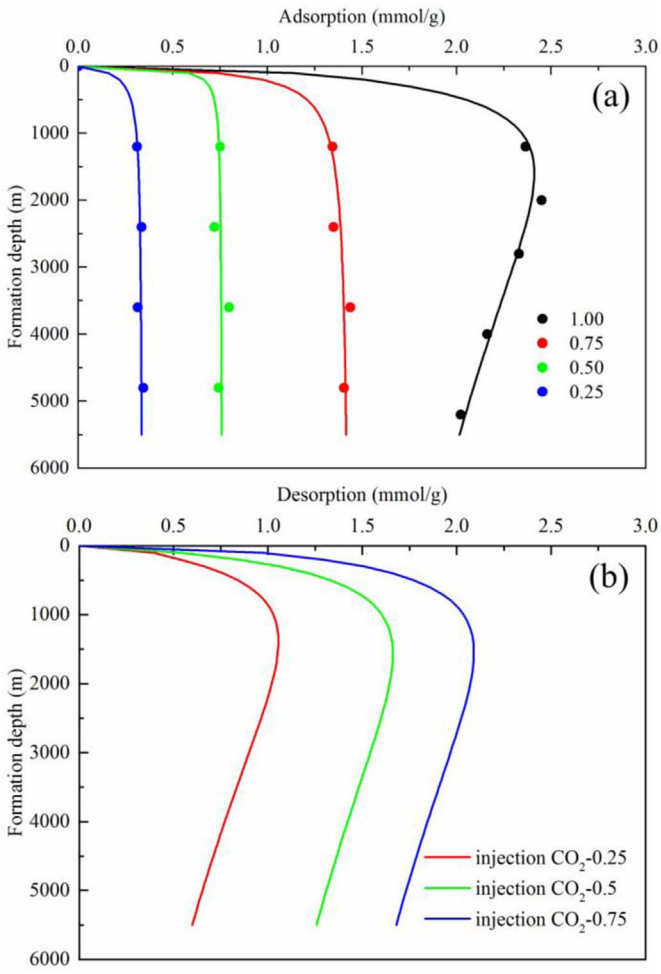

Fig. 9. (a) Adsorption capacity of methane for different methane mole fraction in various buried depth. (b) Desorption amount of methane for the different injection carbon dioxide mole fraction in various buried depth.

recycled into the injection well.

Comparison of methane adsorption capacity and desorption amount for different methane mole fractions in shale formation under geological temperature and pressure conditions as they vary with depth are displays in Fig. 9. The pressure and temperature conditions as a function of depth can be estimated by the pressure gradient (1.0 MPa/100 m) and the geothermal gradient (2.5 °C/100 m). Fig. 9(a) shows that there are significant differences in adsorption capacity for different methane mole fractions in shale formations. The adsorption capacity of pure methane first increases until it reaches maximum at around 2.5 mmol/g and then decreases with the increase of formation depth, whereas the adsorption capacity of methane in carbon dioxide and methane binary mixture first increases quickly and then only shows a slight variation with the increase of formation depth. The temperature effect on adsorption capacity competes with the influence of the pressure. It is generally believed that the adsorption capacity increases with increasing of pressure, but decreases with increasing of temperature. For pure methane, the adsorption capacity first increases as pressure increases, and then the adsorption capacity of methane decreases as formation depth continues to rise. We could infer that at shallow sites of formation, the temperature effect on methane adsorption for the binary mixtures is negligible. Once the site gets deeper, the temperature effect on pure methane adsorption becomes obvious and dominates over the effect of pressure. However, we observe that the adsorption capacity of methane in the binary mixture increases quickly first and then almost stays the same as the formation depth rises. The effects of temperature and pressure on methane adsorption cancel each other out in deep formation. Based on these simulation results, it can be found that when the carbon dioxide purity in shale gas reservoir is larger than 50%, desorption quantity of methane displaced by carbon dioxide can reach 71.3% at the site of 1200 m. Moreover, the desorption quantity of methane in shallow formation is more than that in deep formation. Fig. 9(b) shows the desorption amount of methane for the different injection carbon dioxide mole fraction in various formation depth. In the supercritical carbon dioxide enhanced shale gas development operating process, a promising profit will be obtained when more methane can be desorbed and extracted. Based on the above analysis, the optimal injection depth for supercritical carbon dioxide enhanced shale gas development is 1000–2500 m. To evaluate the optimal injection site more reliably and accurately, influencing injection site factors merits further research.

4. Conclusions

A realistic shale kerogen molecule model is used for GCMC simulations to investigate the adsorption of carbon dioxide and methane binary mixture of different compositions in shale kerogen nanopores in different depth. The model is validated with experimental data and simulation results from literatures. The adsorption of carbon dioxide and methane binary mixture in shale kerogen and the mechanisms significantly affect the design and operation of supercritical carbon dioxide enhanced shale gas development project. It offers a theoretical base for the demonstrated supercritical carbon dioxide enhanced shale gas development in shale kerogen formation, and can be applied to reliably predict adsorption capacity of methane in shale kerogen. Major conclusions are summarized as follows.

1. The adsorption capacity of methane increases with pressure. For methane with 0.75 mol fraction, the adsorption amount is about half of that of pure methane, which indicates that the adsorption capacity decreases quickly at high methane mole fraction. The absolute adsorption amount of carbon dioxide in kerogen exceeds that of methane for all pressure once mole fraction of carbon dioxide is above 0.19.

2. The absolute adsorption capacity of methane decreases as temperature increases, due to the increase of the mean kinetic energy of the methane molecules, which would make the methane escape from the pore walls easier. The adsorption isosteric heat of carbon dioxide is larger than that of methane at the same temperature and pressure. Methane in shale kerogen nanopores is in the higher energy absorption sites whereas carbon dioxide is in the lower energy ones.

3. The adsorption selectivity of carbon dioxide over methane first decreases as pressure increases until pressure reaches critical pressure (7.38 MPa for carbon dioxide), and then stays at around 3.8 as pressure continues to rise. The temperature effect on pure methane adsorption is obvious and dominates over the pressure effect, whereas the effects of temperature and pressure on methane adsorption in the binary mixture cancel each other out in deep formation. The optimal injection depth for supercritical carbon dioxide enhanced shale gas development is 1000–2500 m.

Acknowledgements

This work was supported by the National Natural Science Foundation of China (No. 51674275 and No. 51490652). The authors are grateful for approval to publish this paper.

References

Ambrose, R.J., Clarkson, C.R., Youngblood, J.E., Adams, R., Nguyen, P.D., Nobakht, M., Biseda, B., 2011. Life-cycle decline curve estimation for tight/shale reservoirs. In: SPE Hydraulic Fracturing Technology Conference. Society of Petroleum Engineers.

Behar, F., Vandenbroucke, M., 1987. Chemical modelling of kerogens. Org. Geochem. 11 (1), 15–24.

Bennion, B., Bachu, S., 2008. Drainage and imbibition relative permeability relationships

for supercritical CO2/brine and H2S/brine systems in intergranular sandstone, carbonate, shale, and anhydrite rocks. SPE Reservoir Eval. Eng. 11 (03), 487–496.
Billemont, P., Coasne, B., De Weireld, G., 2010. An experimental and molecular simulation study of the adsorption of carbon dioxide and methane in nanoporous carbons in the presence of water. Langmuir 27 (3), 1015–1024.
Billemont, P., Coasne, B., De Weireld, G., 2013. Adsorption of carbon dioxide, methane, and their mixtures in porous carbons: effect of surface chemistry, water content, and pore disorder. Langmuir 29 (10), 3328–3338.
Bousige, C., Ghimbeu, C.M., Vix-Guterl, C., Pomerantz, A.E., Suleimenova, A., Vaughan, G., Garbarino, G., Feygenson, M., Wildgruber, C., Ulm, F.-J., 2016. Realistic molecular model of kerogen/'s nanostructure. Nat. Mater. 15 (5), 576–582.
Boyer, C., Clark, B., Jochen, V., Lewis, R., Miller, C.K., 2011. Shale gas: a global resource. Oilfield Rev. 23 (3), 28–39.
Brochard, L., Vandamme, M., Pellenq, R.J.-M., Fen-Chong, T., 2012. Adsorption-induced deformation of microporous materials: coal swelling induced by CO2–CH4 competitive adsorption. Langmuir 28 (5), 2659–2670.
Chalmers, G.R., Bustin, R.M., 2007. The organic matter distribution and methane capacity of the Lower Cretaceous strata of Northeastern British Columbia, Canada. Int. J. Coal Geol. 70 (1), 223–239.
Chalmers, G.R., Bustin, R.M., 2008. Lower Cretaceous gas shales in northeastern British Columbia, Part I: geological controls on methane sorption capacity. Bull. Can. Petrol. Geol. 56 (1), 1–21.
Collell, J., Galliero, G., Gouth, F., Montel, F., Pujol, M., Ungerer, P., Yiannourakou, M., 2014. Molecular simulation and modelisation of methane/ethane mixtures adsorption onto a microporous molecular model of kerogen under typical reservoir conditions. Microporous Mesoporous Mater 197, 194–203.
Collell, J., Galliero, G., Vermorel, R., Ungerer, P., Yiannourakou, M., Montel, F., Pujol, M., 2015. Transport of multicomponent hydrocarbon mixtures in shale organic matter by molecular simulations. J. Phys. Chem. 119 (39), 22587–22595.
Curtis, J.B., 2002. Fractured shale-gas systems. AAPG Bull. 86 (11), 1921–1938.
Durand, B., 1980. Kerogen: Insoluble Organic Matter from Sedimentary Rocks (Editions technip). .
Falk, K., Pellenq, R., Ulm, F.J., Coasne, B., 2015. Effect of chain length and pore accessibility on alkane adsorption in kerogen. Energy Fuel. 29 (12), 7889–7896.
Frenkel, D., Smit, B., 2001. Understanding Molecular Simulation: from Algorithms to Applications. Academic press.
Fujita, T., Watanabe, H., Tanaka, S., 2007. Effects of salt addition on strength and dynamics of hydrophobic interactions. Chem. Phys. Lett. 434 (1), 42–48.
Gasparik, M., Bertier, P., Gensterblum, Y., Ghanizadeh, A., Krooss, B.M., Littke, R., 2014. Geological controls on the methane storage capacity in organic-rich shales. Int. J. Coal Geol. 123, 34–51.
Gensterblum, Y., Merkel, A., Busch, A., Krooss, B.M., 2013. High-pressure CH 4 and CO 2 sorption isotherms as a function of coal maturity and the influence of moisture. Int. J. Coal Geol. 118, 45–57.
Gibbs, J.W., 1928. The Collected Works of J. Willard Gibbs, Volume I: Thermodynamics. Yale University Press.
Granato, M.A., Lamia, N., Vlugt, T.J., Rodrigues, A.r.E., 2008. Adsorption equilibrium of isobutane and 1-butene in zeolite 13X by molecular simulation. Ind. Eng. Chem. Res. 47 (16), 6166–6174.
Harris, J.G., Yung, K.H., 1995. Carbon dioxide's liquid-vapor coexistence curve and critical properties as predicted by a simple molecular model. J. Phys. Chem. 99 (31), 12021–12024.
Heller, R., Zoback, M., 2014. Adsorption of methane and carbon dioxide on gas shale and pure mineral samples. J. Unconv. Oil Gas Resour. 8, 14–24.
Howarth, R.W., Santoro, R., Ingraffea, A., 2011. Methane and the greenhouse-gas footprint of natural gas from shale formations. Climatic Change 106 (4), 679–690.
Huang, L., Ning, Z., Wang, Q., Zhang, W., Cheng, Z., Wu, X., Qin, H., 2018. Effect of organic type and moisture on CO 2/CH 4 competitive adsorption in kerogen with implications for CO 2 sequestration and enhanced CH 4 recovery. Appl. Energ 210, 28–43.
Kang, S.M., Fathi, E., Ambrose, R.J., Akkutlu, I.Y., Sigal, R.F., 2011. Carbon dioxide storage capacity of organic-rich shales. SPE J. 16 (04), 842–855.
Kelemen, S., Afeworki, M., Gorbaty, M., Sansone, M., Kwiatek, P., Walters, C., Freund, H., Siskin, M., Bence, A., Curry, D., 2007. Direct characterization of kerogen by X-ray and solid-state 13C nuclear magnetic resonance methods. Energy Fuel. 21 (3), 1548–1561.
Kharaka, Y.K., Cole, D.R., Hovorka, S.D., Gunter, W., Knauss, K.G., Freifeld, B., 2006. Gas-water-rock interactions in Frio Formation following CO2 injection: implications for the storage of greenhouse gases in sedimentary basins. Geology 34 (7), 577–580.
Lee, T., Bocquet, L., Coasne, B., 2016. Activated desorption at heterogeneous interfaces and long-time kinetics of hydrocarbon recovery from nanoporous media. Nat. Commun. 7.
Liu, Y., Wilcox, J., 2012. Effects of surface heterogeneity on the adsorption of CO2 in microporous carbons. Environ. Sci. Technol. 46 (3), 1940–1947.
Lu, X., Jin, D., Wei, S., Zhang, M., Zhu, Q., Shi, X., Deng, Z., Guo, W., Shen, W., 2015. Competitive adsorption of a binary CO 2–CH 4 mixture in nanoporous carbons: effects of edge-functionalization. Nanoscale 7 (3), 1002–1012.
Mao, Z., Sinnott, S.B., 2000. A computational study of molecular diffusion and dynamic flow through carbon nanotubes. J. Phys. Chem. B 104 (19), 4618–4624.
Martin, M.G., Siepmann, J.I., 1998. Transferable potentials for phase equilibria. 1. United-atom description of n-alkanes. J. Phys. Chem. B 102 (14), 2569–2577.
Mastalerz, M., Schimmelmann, A., Lis, G., Drobniak, A., Stankiewicz, A., 2012. Influence of maceral composition on geochemical characteristics of immature shale kerogen: insight from density fraction analysis. Int. J. Coal Geol. 103, 60–69.
McGreevy, R., Pusztai, L., 1988. Reverse Monte Carlo simulation: a new technique for the determination of disordered structures. Mol. Simulat. 1 (6), 359–367.
Mofarahi, M., Bakhtyari, A., 2015. Experimental investigation and thermodynamic modeling of CH4/N2 adsorption on zeolite 13X. J. Chem. Eng. Data 60 (3), 683–696.
Poling, B.E., Prausnitz, J.M., John Paul, O.C., Reid, R.C., 2001. The Properties of Gases and Liquids. McGraw-Hill New York.
Ren, W., Li, G., Tian, S., Sheng, M., Fan, X., 2016. An analytical model for real gas flow in shale nanopores with non-circular cross-section. AIChE J. 62 (8), 2893–2901.
Ren, W., Li, G., Tian, S., Sheng, M., Geng, L., 2017a. Adsorption and surface diffusion of supercritical methane in shale. Ind. Eng. Chem. Res. 56 (12), 3446–3455.
Ren, W., Tian, S., Li, G., Sheng, M., Yang, R., 2017b. Modeling of mixed-gas adsorption on shale using hPC-SAFT-MPTA. Fuel 210, 535–544.
Rexer, T.F., Benham, M.J., Aplin, A.C., Thomas, K.M., 2013. Methane adsorption on shale under simulated geological temperature and pressure conditions. Energy Fuel. 27 (6), 3099–3109.
Rexer, T.F., Mathia, E.J., Aplin, A.C., Thomas, K.M., 2014. High-pressure methane adsorption and characterization of pores in Posidonia shales and isolated kerogens. Energy Fuel. 28 (5), 2886–2901.
Siirola, J.J., 2014. The impact of shale gas in the chemical industry. AIChE J. 60 (3), 810–819.
Sun, H., 1998. COMPASS: an ab initio force-field optimized for condensed-phase applications overview with details on alkane and benzene compounds. J. Phys. Chem. B 102 (38), 7338–7364.
Ungerer, P., Collell, J., Yiannourakou, M., 2014. Molecular modeling of the volumetric and thermodynamic properties of kerogen: influence of organic type and maturity. Energy Fuel. 29 (1), 91–105.
Wang, S., Javadpour, F., Feng, Q., 2016. Fast mass transport of oil and supercritical carbon dioxide through organic nanopores in shale. Fuel 181, 741–758.
Weniger, P., Kalkreuth, W., Busch, A., Krooss, B.M., 2010. High-pressure methane and carbon dioxide sorption on coal and shale samples from the Paraná Basin, Brazil. Int. J. Coal Geol. 84 (3), 190–205.
Xiong, J., Liu, X., Liang, L., Zeng, Q., 2017. Methane adsorption on carbon models of the organic matter of organic-rich shales. Energy Fuel. 31 (2), 1489–1501.
Yaghi, O.M., O'Keeffe, M., Ockwig, N.W., Chae, H.K., Eddaoudi, M., Kim, J., 2003. Reticular synthesis and the design of new materials. Nature 423 (6941), 705–714.
Zhang, J., Liu, K., Clennell, M., Dewhurst, D., Pervukhina, M., 2015. Molecular simulation of CO 2–CH 4 competitive adsorption and induced coal swelling. Fuel 160, 309–317.
Zhang, T., Ellis, G.S., Ruppel, S.C., Milliken, K., Yang, R., 2012. Effect of organic-matter type and thermal maturity on methane adsorption in shale-gas systems. Org. Geochem. 47, 120–131.
Zhao, T., Li, X., Zhao, H., Li, M., 2017. Molecular simulation of adsorption and thermodynamic properties on type II kerogen: influence of maturity and moisture content. Fuel 190, 198–207.